Journal of Sound and Vibration (1998) **212**(5), 781–805

VIBRATION ANALYSIS OF BEAMS WITH MULTIPLE CONSTRAINED LAYER DAMPING PATCHES

S.-W. KUNG AND R. SINGH

Acoustics and Dynamics Laboratory, *Department of Mechanical Engineering*, *The Ohio State University*, *Columbus*, *Ohio* 43210-1107, *USA*

(*Received* 9 *June* 1997, *and in final form* 3 *November* 1997)

A new analytical, energy based approach is described that predicts the harmonic vibration response of a damped beam with multiple viscoelastic patches. Each damping patch consists of a metallic constraining layer and an adhesive viscoelastic layer with spectrally-varying material properties. Since this approach relates all deformation variables in various layers, only flexural shape functions need to be incorporated in the complex eigenvalue problem. Consequently flexural, longitudinal and shear deformation eigenvectors can be calculated. In particular, the shear deformation modes of the viscoelastic core provide useful information regarding the effect of patch damping. The proposed method has been validated by comparing predictions with modal measurements and with those published in the literature. Also, an estimation technique is developed that determines the shear modulus and loss factor properties of two different viscoelastic materials used in experimental studies. An uncertainty study is also performed to establish the error bounds of the estimated material loss factors. Effects of patch boundary conditions, patch cutouts and locations, and mismatched patch combinations are analytically and experimentally examined.

1. INTRODUCTION

Elastic beams with constrained layer viscoelastic material have been analyzed by many investigators, as evident from the studies described in two books on vibration damping by Nashif *et al*. [1] and Sun and Lu [2]. However, much of the prior work has been limited to full coverage, i.e., viscoelastic material added to one or both sides of the beam in a uniform manner. Conversely, only a very few publications have dealt with partially covered sandwich beams [3–6]. Nokes and Nelson [3] were among the earliest investigators to provide an analytical solution to the problem of a partially covered sandwich beam. In their formulation, damped mode shapes are assumed to be the same as the undamped eigenvectors, and the modal loss factor was calculated as the ratio of energy dissipated to the total modal strain energy. A more thorough analytical study was carried out by Lall *et al*. [4]. In their Rayleigh–Ritz approach, both flexural and longitudinal shape functions were incorporated in the eigenvalue problem for a beam with a single damping patch.

In practice, non-uniform and/or partial damping treatment is necessary because of material, thermal, packaging, weight or cost constraints. And in some applications multiple damping patches at selected locations are more desirable. None of the mathematical models, as available in the literature, appears to be directly applicable to this problem. Consequently a clear need exists for a more refined analysis which this article attempts to fulfill. Specific objectives are as follows: (1) develop a new analytical method that considers flexural, longitudinal, rotational and shear deformations in all layers of the sandwich beam, (2) verify the method by comparing results for a single patch with those

0022–460X/98/200781 + 25 $25.00/0/sv971409

reported in the literature by Lall *et al*. [4] and Rao [7], (3) estimate the unknown material properties of viscoelastic material used in the experimental study, (4) validate the method further by comparing predictions with modal measurements on beams with two mismatched patches, and (5) finally examine critical issues such as the patch boundary conditions, a discontinuity in the material (cutout), and mismatched patch combinations. The method is first described for both thin and thick beams where motion variables for all layers are expressed in terms of the flexural displacement of the base structure (i.e., beam). Then the formulation is reduced to a thin beam by employing a Rayleigh–Ritz minimization scheme and an eigenvalue problem of dimension n is obtained where n is the number of admissible functions. This formulation facilitates efficient calculations of various modal deformations in all layers. It should also lead to an improved understanding of damping system designs.

2. ANALYTICAL FORMULATION

2.1. PHYSICAL EXAMPLE

The structure of interest is shown in Figure 1, where N damping patches are attached to the base structure (an elastic beam designated here as layer 3). Each patch p of length l^p is located at x^p. Layer 1 is a metallic layer while layer 2 is an adhesive capable of dissipating vibratory motions. The viscoelastic nature of the second layer is assumed to be linear and frequency dependent. The complex-valued Young's modulus ($\tilde{E}$) and shear modulus ($\tilde{G}$) of the viscoelastic material in patch p are represented by

$$\tilde{E}_2^p(\omega) = E_2^p(\omega)\,(1 + \mathrm{i}\eta_2^p(\omega)), \qquad \tilde{G}_2^p(\omega) = G_2^p(\omega)\,(1 + \mathrm{i}\eta_2^p(\omega)), \tag{1a, b}$$

where $\mathrm{i} = \sqrt{-1}$, η_2^p is the material loss factor and ω is the frequency in rad/s. Note that each patch p may be different in size and material properties.

The scope of this article is limited to the harmonic vibration analysis of a sandwich beam, as shown in Figure 1, with arbitrary boundary conditions. One section of the beam is illustrated in Figure 2 with all relevant variables specified including flexural (w) and longitudinal (u) displacements as well as rotary (ψ) and shear angles (γ). However, shear deformations in elastic layers (layers 1 and 3) will be ignored in section 3 for the sake of simplification.

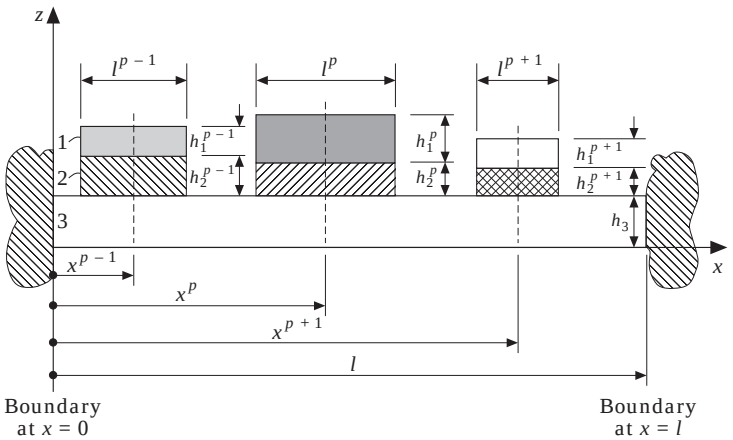

Figure 1. Beam with constrained layer damping patches.

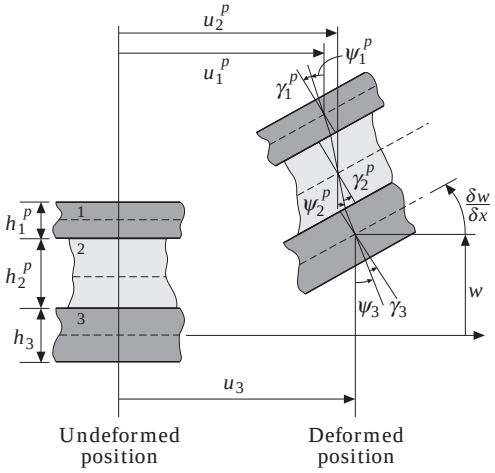

Figure 2. Variables in all layers.

2.2. ENERGY FORMULATION

The complex-valued strain energy ($\tilde{U}$) of the system of Figure 1 has contributions from flexural displacement w (same for each layer), longitudinal displacements u_1^p, u_2^p and u_3, and shear deformation γ_1^p, γ_2^p and γ_3 where superscript $p = 1, \ldots, N$ denotes the patch number for layers 1 and 2. Also, refer to Appendix A for the identification of symbols.

$$\tilde{U}(\omega) = \sum_{p=1}^{N} \int_p [\tfrac{1}{2} (\mathscr{D}\mathbf{r}_1^p)^{\mathrm{T}} \mathbf{E}_1^p (\mathscr{D}\mathbf{r}_1^p) + \tfrac{1}{2} (\mathscr{D}\mathbf{r}_2^p)^{\mathrm{T}} \tilde{\mathbf{E}}_2^p (\omega) (\mathscr{D}\mathbf{r}_2^p)] \, \mathrm{d}x + \int_0^l \tfrac{1}{2} (\mathscr{D}\mathbf{r}_3)^{\mathrm{T}} \mathbf{E}_3 (\mathscr{D}\mathbf{r}_3) \, \mathrm{d}x. \quad (2)$$

Note that $\mathbf{r}_1^p$, $\mathbf{r}_2^p$, and $\mathbf{r}_3$ are deformation vectors in which rotations ψ_1^p, ψ_2^p, and ψ_3 are used instead of shear deformations γ_1^p, γ_2^p, and γ_3:

$$\mathbf{r}_1^p = \begin{bmatrix} w \\ \psi_1^p \\ u_1^p \end{bmatrix}, \qquad \mathbf{r}_2^p = \begin{bmatrix} w \\ \psi_2^p \\ u_2^p \end{bmatrix}, \qquad \mathbf{r}_3 = \begin{bmatrix} w \\ \psi_3 \\ u_3 \end{bmatrix}; \qquad p = 1, \ldots, N. \quad (3a\text{–}c)$$

Here $\mathscr{D}$ is the differential operator matrix defined as

$$\mathscr{D} = \begin{bmatrix} \partial^2/\partial x^2 & 0 & 0 \\ \partial/\partial x & -1 & 0 \\ 0 & 0 & \partial/\partial x \end{bmatrix}. \quad (4)$$

And $\mathbf{E}_1^p$, $\tilde{\mathbf{E}}_2^p$ and $\mathbf{E}_3$ are elasticity matrices that are defined as

$$\mathbf{E}_1^p = \begin{bmatrix} E_1^p I_1^p & 0 & 0 \\ 0 & \kappa G_1^p A_1^p & 0 \\ 0 & 0 & E_1^p A_1^p \end{bmatrix}, \qquad \tilde{\mathbf{E}}_2^p (\omega) = \begin{bmatrix} \tilde{E}_2^p (\omega) I_2^p & 0 & 0 \\ 0 & \kappa \tilde{G}_2^p (\omega) A_2^p & 0 \\ 0 & 0 & \tilde{E}_2^p (\omega) A_2^p \end{bmatrix},$$

$$\mathbf{E}_3 = \begin{bmatrix} E_3 I_3 & 0 & 0 \\ 0 & \kappa G_3 A_3 & 0 \\ 0 & 0 & E_3 A_3 \end{bmatrix}; \qquad p = 1, \ldots, N, \quad (5a\text{–}c)$$

where κ is the shear correction factor. The real-valued kinetic energy of the system (T) due to flexural, longitudinal and rotary motions is expressed as

$$T = \sum_{p=1}^{N} \int_{p} [\tfrac{1}{2}\dot{\mathbf{r}}_1^{p\mathrm{T}}\mathbf{H}_1\dot{\mathbf{r}}_1^{p} + \tfrac{1}{2}\dot{\mathbf{r}}_2^{p\mathrm{T}}\mathbf{H}_2\dot{\mathbf{r}}_2^{p}]\,\mathrm{d}x + \int_0^l \tfrac{1}{2}\dot{\mathbf{r}}_3^{\mathrm{T}}\mathbf{H}_3\dot{\mathbf{r}}_3\,\mathrm{d}x, \tag{6}$$

where

$$\mathbf{H}_1^p = \begin{bmatrix} \rho_1^p A_1^p & 0 & 0 \\ 0 & \rho_1^p I_1^p & 0 \\ 0 & 0 & \rho_1^p A_1^p \end{bmatrix}, \qquad \mathbf{H}_2^p = \begin{bmatrix} \rho_2^p A_2^p & 0 & 0 \\ 0 & \rho_2^p I_2^p & 0 \\ 0 & 0 & \rho_2^p A_2^p \end{bmatrix},$$

$$\mathbf{H}_3 = \begin{bmatrix} \rho_3 A_3 & 0 & 0 \\ 0 & \rho_3 I_3 & 0 \\ 0 & 0 & \rho_3 A_3 \end{bmatrix}, \qquad p = 1, \ldots, N. \tag{7a–c}$$

2.3. RAYLEIGH–RITZ METHOD

To implement the Rayleigh–Ritz minimization scheme, the flexural displacement of the beam w is approximated as

$$w(x, t) = \boldsymbol{\varphi}(x)\mathbf{q}(t), \tag{8}$$

where $\mathbf{q} = [q_1\ q_2\ \cdots\ q_k\ \cdots\ q_n]^{\mathrm{T}}$ is the generalized displacement vector of the system and $\boldsymbol{\varphi} = [\phi_1\ \phi_2\ \cdots\ \phi_k\ \cdots\ \phi_n]$ is the flexural shape function vector in which each term ϕ_k is an admissible function that satisfies the essential boundary conditions of the beam.

Recall that energy equations (2) and (6) contain $4N + 3$ unknowns: flexural displacement w, rotation ψ_1^p, ψ_2^p, and ψ_3, and longitudinal displacements u_1^p, u_2^p, and u_3 for $p = 1, \ldots, N$. If these unknowns were to be approximated with n trial functions and to be incorporated in the Rayleigh–Ritz minimization scheme, the resulting eigenvalue problem would be of dimension $n(4N + 3)$. An alternative is to assume relationships between these unknowns; that is, for each flexural admissible function $\phi_k(x)$, the corresponding rotational shape functions $\xi_{1,k}^p(x)$, $\xi_{2,k}^p(x)$ and $\xi_{3,k}(x)$ as well as the longitudinal shape functions $\varsigma_{1,k}^p(x)$, $\varsigma_{2,k}^p(x)$ and $\varsigma_{3,k}(x)$ can be calculated by using these relationships, which will be derived in section 3. With the above assumption, deformation vectors can be expressed as

$$\mathbf{r}_1^p = \mathbf{S}_1^p(x)\mathbf{q}(t), \qquad \mathbf{r}_2^p = \mathbf{S}_2^p(x)\mathbf{q}(t), \qquad \mathbf{r}_3 = \mathbf{S}_3(x)\mathbf{q}(t), \tag{9a–c}$$

where $\mathbf{S}_1^p$, $\mathbf{S}_2^p$, and $\mathbf{S}_3$ are admissible shape function matrices defined as

$$\mathbf{S}_1^p = \begin{bmatrix} \boldsymbol{\varphi} \\ \boldsymbol{\xi}_1^p \\ \boldsymbol{\varsigma}_1^p \end{bmatrix}, \qquad \mathbf{S}_2^p = \begin{bmatrix} \boldsymbol{\varphi} \\ \boldsymbol{\xi}_2^p \\ \boldsymbol{\varsigma}_2^p \end{bmatrix}, \qquad \mathbf{S}_3 = \begin{bmatrix} \boldsymbol{\varphi} \\ \boldsymbol{\xi}_3 \\ \boldsymbol{\varsigma}_3 \end{bmatrix}; \qquad \text{for } p = 1, \ldots, N; \tag{10a–c}$$

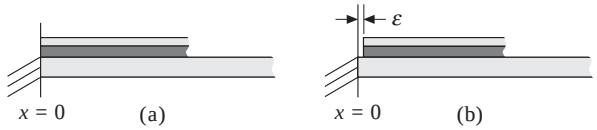

Figure 3. Patch boundary conditions at $x = 0$. (a) Fixed-end patch, (b) free-end patch where $\varepsilon \to 0$.

and $\boldsymbol{\xi}_1^p = [\xi_{1,1}^p \ \cdots \ \xi_{1,k}^p \ \cdots \ \xi_{1,n}^p]$, $\boldsymbol{\xi}_2^p = [\xi_{2,1}^p \ \cdots \ \xi_{2,k}^p \ \cdots \ \xi_{2,n}^p]$, $\boldsymbol{\xi}_3 = [\xi_{3,1} \ \cdots \ \xi_{3,k} \ \cdots \ \xi_{3,n}]$, are the corresponding rotational shape function vectors while $\boldsymbol{\varsigma}_1^p = [\varsigma_{1,1}^p \ \cdots \ \varsigma_{1,k}^p \ \cdots \ \varsigma_{1,n}^p]$, $\boldsymbol{\varsigma}_2^p = [\varsigma_{2,1}^p \ \cdots \ \varsigma_{2,k}^p \ \cdots \ \varsigma_{2,n}^p]$, $\boldsymbol{\varsigma}_3 = [\varsigma_{3,1} \ \cdots \ \varsigma_{3,k} \ \cdots \ \varsigma_{3,n}]$ are the corresponding longitudinal shape function vectors. Using equation (9), the strain and kinetic energies can be written as

$$\tilde{U}(\omega) = \tfrac{1}{2}\,\mathbf{q}^{\mathrm{T}}\tilde{\mathbf{K}}(\omega)\mathbf{q}, \qquad T = \tfrac{1}{2}\,\dot{\mathbf{q}}^{\mathrm{T}}\mathbf{M}\dot{\mathbf{q}}, \tag{11a, b}$$

where the frequency dependent complex-valued stiffness ($\tilde{\mathbf{K}}$) and real-valued mass ($\mathbf{M}$) matrices of the system are

$$\tilde{\mathbf{K}}(\omega) = \sum_{p=1}^{N} \int_p [(\mathscr{D}\mathbf{S}_1^p)^{\mathrm{T}}\mathbf{E}_1\,(\mathscr{D}\mathbf{S}_1^p) + (\mathscr{D}\mathbf{S}_2^p)^{\mathrm{T}}\tilde{\mathbf{E}}_2\,(\omega)\,(\mathscr{D}\mathbf{S}_2^p)]\,\mathrm{d}x + \int_0^l (\mathscr{D}\mathbf{S}_3)^{\mathrm{T}}\mathbf{E}_3\,(\mathscr{D}\mathbf{S}_3)\,\mathrm{d}x,$$

$$\mathbf{M} = \sum_{p=1}^{N} \int_p [\mathbf{S}_1^{p^{\mathrm{T}}}\mathbf{H}_1\,\mathbf{S}_1^p + \mathbf{S}_2^{p^{\mathrm{T}}}\mathbf{H}_2\,\mathbf{S}_2^p]\,\mathrm{d}x + \int_0^l \mathbf{S}_3^{\mathrm{T}}\mathbf{H}_3\,\mathbf{S}_3\,\mathrm{d}x. \tag{12a, b}$$

The frequency dependent complex eigenvalue problem of dimension n can be obtained as

$$\mathbf{M}\ddot{\mathbf{q}} + \tilde{\mathbf{K}}(\omega)\mathbf{q} = \mathbf{0}. \tag{13}$$

Several approaches are available in the literature [9, 10] for solving eigenvalue problems of non-proportionally damped systems with frequency dependent parameters, whose eigenvalues and eigenvectors are complex-valued. Using the method of Rikards *et al*. [10], undamped natural frequencies (ω_r) and composite modal loss factors (η_r) are related to the complex-valued eigenvalues $\tilde{\lambda}_r$ of equation (13) in the following manner where r is the modal index:

$$\omega_r = \sqrt{\mathrm{Re}\,(\tilde{\lambda}_r)}, \qquad \eta_r = \mathrm{Im}\,(\tilde{\lambda}_r)/\mathrm{Re}\,(\tilde{\lambda}_r); \qquad r = 1, \ldots, n. \tag{14a, b}$$

TABLE 1

System parameters used for examples given in the literature. Refer to Figure 1 *for nomenclature*

		Rao [7]	Lall *et al*. [4]
Material properties	E_1 and E_3 (Pa)	206×10^9	207×10^9
	G_2 (Pa)	$9{\cdot}8 \times 10^9$	$2{\cdot}615 \times 10^5$
	η_2	0·1	0·38
	ρ_1 and ρ_3 (kg/m^3)	7850	7800
	ρ_2 (kg/m^3)	2600	2000
Dimensions (mm)	h_1	3	0·5
	h_2	5	2·5
	h_3	8	5
	l	100	300
Beam boundary conditions		Clamped-free	Simply supported on both sides
Patch boundary conditions at $x = 0$		fixed end	free end

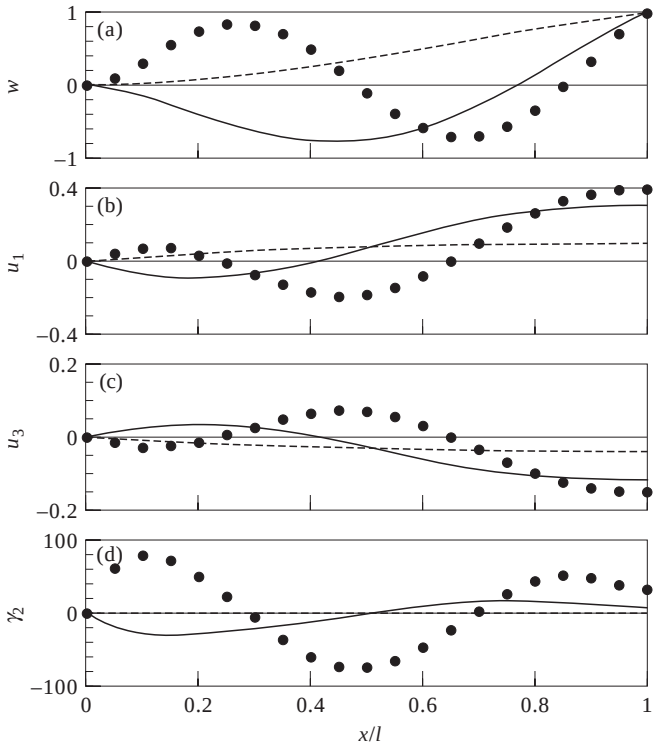

Figure 4. First three mode shapes for Rao's example [7]. (a) Flexural modes (w) of the beam, (b) longitudinal modes (u_1) of layer 1, (c) longitudinal modes (u_3) of layer 3, (d) shear modes (γ_2) of layer 2. Key: ---, mode 1; ——, mode 2; ●, mode 3.

3. ADMISSIBLE FUNCTIONS FOR THIN BEAMS

In section 2.3, the fundamental relationships between all $4N + 3$ unknowns are assumed in order to obtain an eigenvalue problem of dimension n. This section explicitly shows these relationships by deriving the corresponding shape function of each unknown for a given admissible flexural function. For the sake of simplification, only thin elastic layers (1 and 3) are assumed. The following two steps are involved in the variable reduction procedure. First, the classic sandwich beam theory [7] is employed along with the thin elastic layer assumption to reduce the number of unknowns to $N + 2$. Second, a secondary

TABLE 2

Comparison between Rao's published [7] *and proposed methods. See Table* 1 *for parameters*

	Natural frequency (Hz)		Modal loss factor	
	Published	Proposed	Published	Proposed
Mode 1	1309 (1320)*	1310	$7{\cdot}0 \times 10^{-3}$ ($6{\cdot}8 \times 10^{-3}$)*	$7{\cdot}0 \times 10^{-3}$
Mode 2	– (6869)*	6986	– ($2{\cdot}7 \times 10^{-2}$)*	$2{\cdot}8 \times 10^{-2}$
Mode 3	– (16 497)*	16 854	– ($3{\cdot}8 \times 10^{-2}$)*	$3{\cdot}7 \times 10^{-2}$

* Solution from an approximate formulation given by Rao [7]

TABLE 3

Comparison between Lall et al.'s published [4] *and proposed methods. See Table* 1 *for parameters*

	Natural frequency (rad/s)		Modal loss factor	
	Published	Proposed	Published	Proposed
20% coverage				
Mode 1	811	811	$6{\cdot}1 \times 10^{-6}$	$6{\cdot}3 \times 10^{-6}$
40% coverage				
Mode 1	789	788	$1{\cdot}7 \times 10^{-4}$	$1{\cdot}7 \times 10^{-4}$
60% coverage				
Mode 1	759	759	$9{\cdot}3 \times 10^{-4}$	$9{\cdot}5 \times 10^{-4}$
100% coverage				
Mode 1	741	741	$4{\cdot}5 \times 10^{-3}$	$4{\cdot}5 \times 10^{-3}$
Mode 2	2948	2949	$1{\cdot}1 \times 10^{-3}$	$1{\cdot}1 \times 10^{-3}$
Mode 3	6630	6630	$5{\cdot}1 \times 10^{-4}$	$5{\cdot}1 \times 10^{-4}$
Mode 4	11 783	11 783	$2{\cdot}9 \times 10^{-4}$	$2{\cdot}9 \times 10^{-4}$

minimization scheme is used to further reduce the $N + 2$ unknowns to one flexural shape function vector $\boldsymbol{\varphi}$.

3.1. VARIABLE REDUCTION BY USING CLASSIC SANDWICH BEAM THEORY

Kerwin's weak core assumption [8] is applied to longitudinal shape functions ς_1^p and ς_3 as

$$E_1^p A_1^p \, \partial \varsigma_{1,k}^p / \partial x + E_3 A_3 \, \partial \varsigma_{3,k} / \partial x = 0; \qquad p = 1, \ldots, N. \tag{15}$$

Integrating both sides with respect to x, the following expression is obtained:

$$\varsigma_{1,k}^p = d_k^p - e^p \varsigma_{3,k}, \tag{16}$$

where $e^p = E_3 A_3 / (E_1^p A_1^p)$ and d_k^p is the constant that relates admissible shape $\varsigma_{3,k}$ to the corresponding $\varsigma_{1,k}^p$.

Next, observing the kinematic relationship in Figure 2, the longitudinal deformation ($\varsigma_{2,k}^p$) and rotation ($\xi_{2,k}^p$) of layer 2 are expressed as

$$\varsigma_{2,k}^p = \tfrac{1}{2} [(\varsigma_{3,k} - (h_3/2)\xi_{3,k}) + (\varsigma_{1,k}^p + (h_1^p/2)\xi_{1,k}^p)], \tag{17}$$

$$\xi_{2,k}^p = (1/h_2) [(\varsigma_{3,k} - (h_3/2)\xi_{3,k}) - (\varsigma_{1,k}^p + (h_1^p/2)\xi_{1,k}^p)]. \tag{18}$$

Substituting equation (16) into equations (17, 18), $\varsigma_{2,k}^p$ and $\xi_{2,k}^p$ are rewritten as

$$\varsigma_{2,k}^p = (h_1^p/4)\xi_{1,k}^p - (h_3/4)\xi_{3,k} + ([1 - e^p]/2)\varsigma_{3,k} + (1/2)d_k^p, \tag{19}$$

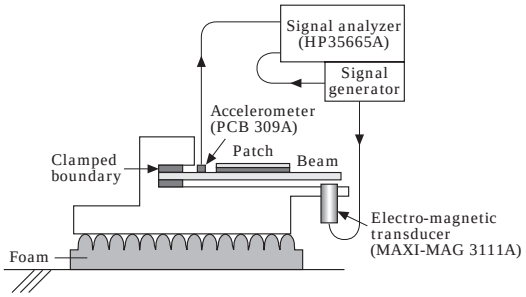

Figure 5. Schematic of experimental setup.

TABLE 4

Properties of baseline beam and damping patches

		Stiffness (N/m^2)	Density (kg/m^3)	Thickness
Patch A	Layer 1	$E_1 = 180 \times 10^9$	$\rho_1 = 7720$	$h_1/l = 4{\cdot}43 \times 10^{-3}$
	Layer 2	$G_2 = 0{\cdot}25 \times 10^6$	$\rho_2 = 2000$	$h_2/l = 2{\cdot}86 \times 10^{-4}$
Patch B	Layer 1	$E_1 = 180 \times 10^9$	$\rho_1 = 7720$	$h_1/l = 2{\cdot}43 \times 10^{-3}$
	Layer 2	$G_2 = 3 \times 10^6$	$\rho_2 = 2000$	$h_2/l = 2{\cdot}86 \times 10^{-4}$
Baseline beam of $l = 177{\cdot}8$ mm	Layer 3	$E_3 = 180 \times 10^9$	$\rho_3 = 7350$	$h_3/l = 8{\cdot}29 \times 10^{-3}$

$$\xi^p_{2,k} = -(h^p_1/2h^p_2)\xi^p_{1,k} - (h_3/2h^p_2)\xi_{3,k} + ([1+e^p]/h^p_2)\varsigma_{3,k} - (1/h^p_2)d^p_k. \tag{20}$$

For a beam with thin elastic layers whose shear deformations γ^p_1 and γ_3 are ignored, rotations of layer 1 and layer 3 are the same as the slope of the beam,

$$\xi^p_{1,k} = \partial\phi_k/\partial x, \qquad \xi_{3,k} = \partial\phi_k/\partial x. \tag{21a, b}$$

Therefore, $\varsigma^p_{2,k}$ and $\xi^p_{2,k}$ can be rewritten as

$$\varsigma^p_{2,k} = ([h^p_1 - h_3]/4)\ \partial\phi_k/\partial x + ([1-e^p]/2)\varsigma_{3,k} + (1/2)d^p_k, \tag{22}$$

$$\xi^p_{2,k} = -([h^p_1 + h_3]/2h^p_2)\partial\phi_k/\partial x + ([1+e^p]/h^p_2)\varsigma_{3,k} - (1/h^p_2)d^p_k. \tag{23}$$

To reduce the $4N+3$ unknowns to $N+2$, define transfer matrices $\mathbf{V}_1$, $\mathbf{V}_2$ and $\mathbf{V}_3$ as

$$\mathbf{S}^p_1 = \mathbf{V}^p_1\,\mathbf{\Phi}^p, \qquad \mathbf{S}^p_2 = \mathbf{V}^p_2\,\mathbf{\Phi}^p, \qquad \mathbf{S}_3 = \mathbf{V}_3\,\mathbf{\Phi}, \tag{24a–c}$$

where transfer matrices $\mathbf{V}^p_1$, $\mathbf{V}^p_2$, and $\mathbf{V}_3$, as shown below, are derived by using equations (16, 21–23):

$$\mathbf{V}^p_1 = \begin{bmatrix} 1 & 0 & 0 \\ \dfrac{\partial}{\partial x} & 0 & 0 \\ 0 & -e^p & 1 \end{bmatrix}, \qquad \mathbf{V}^p_2 = \begin{bmatrix} 1 & 0 & 0 \\ \dfrac{-(h^p_1+h_3)}{2h^p_2}\dfrac{\partial}{\partial x} & \dfrac{(e^p+1)}{h^p_2} & -\dfrac{1}{h^p_2} \\ \dfrac{(h^p_1-h_3)}{4}\dfrac{\partial}{\partial x} & \dfrac{1-e^p}{2} & \dfrac{1}{2} \end{bmatrix},$$

$$\mathbf{V}_3 = \begin{bmatrix} 1 & 0 \\ \dfrac{\partial}{\partial x} & 0 \\ 0 & 1 \end{bmatrix}. \tag{25a–c}$$

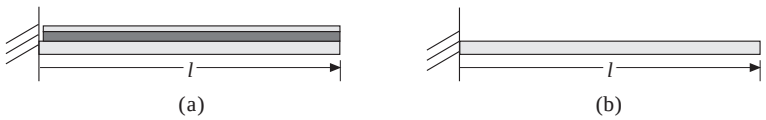

(a) (b)

Figure 6. Benchmark examples. (a) Full free-end patch (benchmark for damping studies based on experimental measurements), (b) beam without any patch (baseline beam).

TABLE 5

Benchmark results for cantilever beams

Mode r	Undamped natural frequency						Modal loss factor			
	Theory			Experiment*			Theory		Experiment*	
	f_r (Hz)	$(\beta_r l)^2$	$\hat{\omega}_r$ (%)	f_r (Hz)	$(\beta_r l)^2$	$\hat{\omega}_r$ (%)	η_r (%)	$\hat{\eta}_r$ (%)	η_r (%)	$\hat{\eta}_r$ (%)
(a) Beam with full free end Patch A										
1	34	3·6	115	30	2·8	100	11	100	11	100
2	219	20·7	95	230	21·7	100	27	100	27	100
3	580	54·7	96	601	56·8	100	23	100	23	100
4	1117	105·4	99	1125	106·2	100	17	100	17	100
5	1834	173·1	99	1850	174·6	100	16	100	16	100
(b) Baseline beam (without any patch)										
1	37	3·5	125	36	3·4	120	0	0	1·6	14·9
2	233	22·0	102	231	21·8	101	0	0	0·1	0·5
3	654	61·7	109	695	65·6	116	0	0	0·1	0·3
4	1281	120·9	114	1254	118·3	111	0	0	0·1	0·5
5	2118	199·9	114	2050	193·5	111	0	0	0·1	0·6

* Experimental database for the full free-end patch is the benchmark case

Also, the reduced admissible shape matrices $\mathbf{\Phi}^p$ and $\mathbf{\Phi}$ of equation (24) are defined as

$$\mathbf{\Phi}^p = \begin{bmatrix} \boldsymbol{\varphi} \\ \boldsymbol{\varsigma}_3 \\ \mathbf{d}^p \end{bmatrix}, \qquad \mathbf{\Phi} = \begin{bmatrix} \boldsymbol{\varphi} \\ \boldsymbol{\varsigma}_3 \end{bmatrix}; \qquad p = 1, \ldots, N, \tag{26a, b}$$

where $\mathbf{d}^p = [d_1^p \ \cdots \ d_k^p \ \cdots \ d_n^p]$ and each term d_k^p is a constant that relates the admissible shape $\varsigma_{3,k}$ to its corresponding $\varsigma_{1,k}^p$. Note that this constant (d_k^p) has been ignored by many prior researchers but it is retained here since it plays an important role in determining the longitudinal boundary conditions [11] for each patch. For example, if patch p is a fixed-end patch as shown in Figure 3(a), $\mathbf{d}^p$ must be zero and accordingly it must be eliminated from $\mathbf{\Phi}^p$. As for a free-end patch of Figure 3(b), $\mathbf{d}^p$ remains undetermined until the secondary minimization scheme is used. The issue of patch boundary conditions will be further examined in section 5.1.

3.2. VARIABLE REDUCTIONS BY USING A SECONDARY MINIMIZATION SCHEME

Recall that the number of unknowns has been reduced from $4N + 3$ to $N + 2$ for the kth admissible function set in matrices $\mathbf{\Phi}^p$ and $\mathbf{\Phi}$. These $N + 2$ unknowns are flexural shape functions ϕ_k, longitudinal shape functions for the base beam $\varsigma_{3,k}$, and the constants d_k^p. Since no explicit equations are available to relate these unknowns, a secondary minimization scheme is implemented. First, each admissible function $\varsigma_{3,k}$ is approximated as

$$\varsigma_{3,k} = \boldsymbol{\chi}\mathbf{c}_k, \tag{27}$$

where $\mathbf{c}_k$ is a coefficient vector to be determined and $\boldsymbol{\chi}$ is the row trial function vector whose terms satisfy essential boundary conditions. The real part of total strain energy of the beam (U_k) experiencing the deformations of the kth of admissible function set $\mathbf{\Phi}_k^p$ and $\mathbf{\Phi}_k$ can be expressed as

$$U_k(\omega) = \tfrac{1}{2} K_k(\omega) q_k^2, \tag{28}$$

where

$$K_k(\omega) = \sum_{p=1}^{N} \int_p [(\mathscr{D}\mathbf{V}_1^p \boldsymbol{\Phi}_k^p)^{\mathrm{T}} \mathbf{E}_1 (\mathscr{D}\mathbf{V}_1^p \boldsymbol{\Phi}_k^p) + (\mathscr{D}\mathbf{V}_2^p \boldsymbol{\Phi}_k^p)^{\mathrm{T}} \tilde{\mathbf{E}}_2^p(\omega) (\mathscr{D}\mathbf{V}_2^p \boldsymbol{\Phi}_k^p)\, \mathrm{d}x$$

$$+ \int_0^l (\mathscr{D}\mathbf{V}_3 \boldsymbol{\Phi}_k)^{\mathrm{T}} \mathbf{E}_3 (\mathscr{D}\mathbf{V}_3 \boldsymbol{\Phi}_k)\, \mathrm{d}x \tag{29}$$

is the effective stiffness at any ω of interest and q_k is the corresponding generalized displacement. Note that in the above analysis the imaginary part of the complex-valued stiffness is ignored because only kinematic relationships are of interest. By substituting equations (25–27, 29) into equation (28) and minimizing U_k with respect to coefficients of $\mathbf{c}_k$ and $\mathbf{d}_k$, where $\mathbf{d}_k = [d_k^1 \cdots d_k^p \cdots d_k^N]^{\mathrm{T}}$, the set of governing equations can be summarized in matrix form as

$$\mathbf{A}\mathbf{C}_k = \mathbf{B}_k, \tag{30}$$

where

$$\mathbf{A} = \begin{bmatrix} \mathbf{A}^{cc} & \mathbf{A}^{cd} \\ \mathbf{A}^{dc} & \mathbf{A}^{dd} \end{bmatrix}, \qquad \mathbf{B}_k = \begin{bmatrix} \mathbf{B}_k^c \\ \mathbf{B}_k^d \end{bmatrix}, \qquad \mathbf{C}_k = \begin{bmatrix} \mathbf{c}_k \\ \mathbf{d}_k \end{bmatrix}. \tag{31a–c}$$

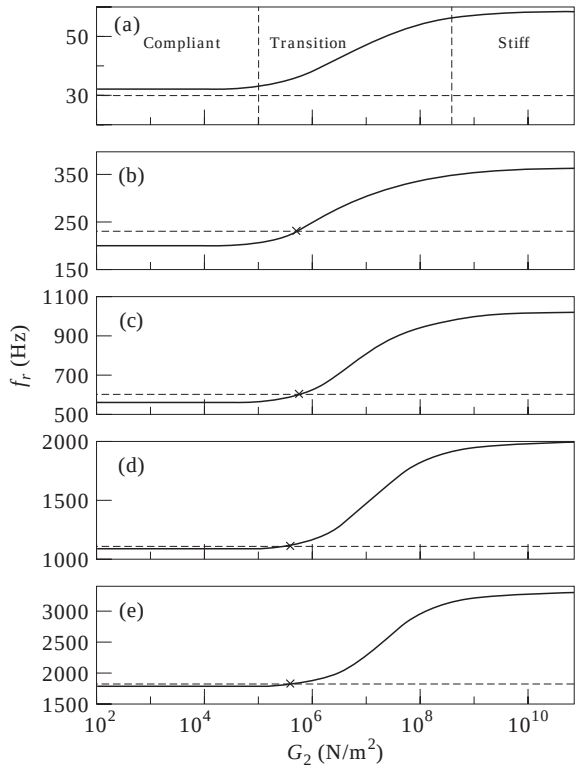

Figure 7. Predicted f_r–G_2 relationships and measured f_r values for estimating G_2 value. (a) Mode 1, (b) mode 2, (c) mode 3, (d) mode 4, (e) mode 5. Key: ——, theory; – – –, experiment; ×, intersection.

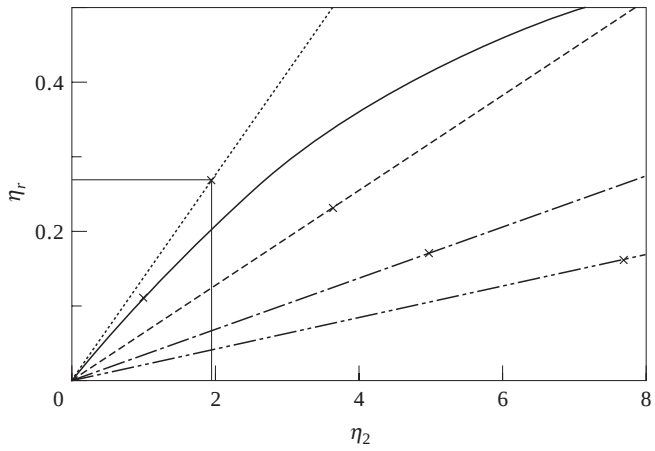

Figure 8. Predicted η_r–η_2 relationships and measured η_r values for estimating η_2 value. Key: ——, mode 1; · · ·, mode 2; ---, mode 3; — · —, mode 4; — · · —, mode 5; ×, measurements.

Submatrices of $\mathbf{A}$ and sub-vectors of $\mathbf{B}_k$ are obtained as follows:

$$\mathbf{A}^{cc} = \int_0^l \left(\frac{\partial}{\partial x}\boldsymbol{\chi}\right)^{\mathrm{T}} E_3 A_3 \left(\frac{\partial}{\partial x}\boldsymbol{\chi}\right) \mathrm{d}x + \sum_{p=1}^{N} \int_p \left[\left(\frac{\partial}{\partial x}\boldsymbol{\chi}\right)^{\mathrm{T}} E_3 A_3 e^p \left(\frac{\partial}{\partial x}\boldsymbol{\chi}\right) + \boldsymbol{\chi}^{\mathrm{T}} \frac{(e^p+1)^2 G_2^p A_2}{(h_2^p)^2}\boldsymbol{\chi}\right] \mathrm{d}x,$$

$$\mathbf{A}^{cd} = -\left[\frac{(e^1+1)G_2^1 A_2^1}{(h_2^1)^2}\int_1 \boldsymbol{\chi}^{\mathrm{T}}\,\mathrm{d}x \quad \cdots \quad \frac{(e^p+1)G_2^p A_2^p}{(h_2^p)^2} \times \int_p \boldsymbol{\chi}^{\mathrm{T}}\,\mathrm{d}x \quad \cdots \quad \frac{(e^N+1)G_2^N A_2^N}{(h_2^N)^2}\int_N \boldsymbol{\chi}^{\mathrm{T}}\,\mathrm{d}x\right],$$

$$\mathbf{A}^{dc} = -\left[\frac{(e^1+1)G_2^1 A_2^1}{(h_2^1)^2}\int_1 \boldsymbol{\chi}^{\mathrm{T}}\,\mathrm{d}x \quad \cdots \quad \frac{(e^p+1)G_2^p A_2^p}{(h_2^p)^2}\right.$$

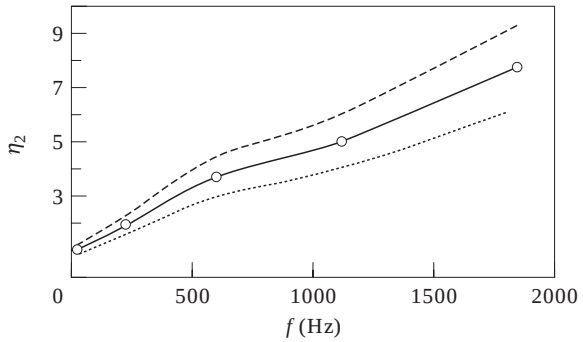

Figure 9. Frequency dependent material loss factor η_2 for layer 2 of patch A. Key: —○—, assumed mean; ---, upper limit; · · ·, lower limit.

$$\times \int_p \boldsymbol{\chi}^{\mathrm{T}}\,\mathrm{d}x \quad \cdots \quad \frac{(e^N+1)G_2^N A_2^N}{(h_2^N)^2}\int_N \boldsymbol{\chi}^{\mathrm{T}}\,\mathrm{d}x\Bigg]^{\mathrm{T}},$$

$$\mathbf{A}^{dd} = \begin{bmatrix} G_2^1 A_2^1 l^1/(h_2^1)^2 & & & & \\ & \ddots & & \mathbf{0} & \\ & & G_2^p A_2^p l^p/(h_2^p)^2 & & \\ & \mathbf{0} & & \ddots & \\ & & & & G_2^N A_2^N l^N/(h_2^N)^2 \end{bmatrix},$$

$$\mathbf{B}_k^c = \sum_{p=1}^{N}\int_p \frac{C^p(e^p+1)G_2^p A_2^p}{(h_2^p)^2}\left(\frac{\partial\phi_k}{\partial x}\right)\boldsymbol{\chi}^{\mathrm{T}}\,\mathrm{d}x,$$

$$\mathbf{B}_k^d = -\left[\frac{C^1(e^1+1)G_2^1 A_2^1}{(h_2^1)^2}\vartheta^1\phi_k \quad \cdots \quad \frac{C^p(e^p+1)G_2^p A_2^p}{(h_2^p)^2}\vartheta^p\phi_k \quad \cdots \quad \frac{C^N(e^N+1)G_2^N A_2^N}{(h_2^N)^2}\vartheta^N\phi_k\right]^{\mathrm{T}},$$

(32a–f)

where $C^p = (h_1^p + 2h_2^p + h_3)/2$ and the spatial operator ϑ^p is defined as

$$\vartheta^p f(x) = f(x^p + l^p/2) - f(x^p - l^p/2). \tag{33}$$

The coefficients $\mathbf{c}_k$ and $\mathbf{d}_k$ of $\mathbf{C}_k$ can be calculated by

$$\mathbf{C}_k = \mathbf{A}^{-1}\mathbf{B}_k, \tag{34}$$

provided $|\mathbf{A}| \neq 0$. As a result, reduced admissible shape matrices $\boldsymbol{\Phi}^p$ and $\boldsymbol{\Phi}$ can be determined for a given flexural shape function vector $\boldsymbol{\varphi}$.

4. COMPARISON WITH LITERATURE

To validate the proposed formulations, two specific examples found in the existing literature are analyzed first. Table 1 summarizes the system parameters that were used by Rao [7] and Lall *et al*. [4]. For the present study, analytical solutions are obtained by using

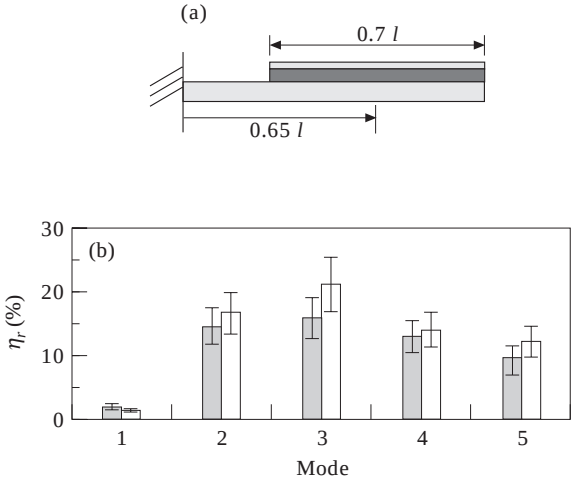

Figure 10. Comparisons of measurements and predictions of cantilever sandwich beam with a single patch. (a) Schematic, (b) modal loss factors. Key: ▨, experiment; □, theory; I, variation.

20 admissible functions for the flexural displacement and 20 trial longitudinal shape functions for each flexural shape function.

Rao [7] studied a clamped–free beam with a full damping treatment on one side of the beam. The viscoelastic material has a fixed boundary condition at $x = 0$. He found the exact solution only for the first mode. Additionally, the first three natural frequencies and modal loss factors were calculated by using an approximate formulation [7]. It is seen in Table 2 that the results obtained from the present method are very close to the exact solutions given by Rao. Reasonable agreement is also seen with Rao's approximations.

Lall *et al*. [4] analyzed a simply supported beam with a single patch. The following parametric studies were carried out: coverage ratios $l^p/l = 20$, 40, 60 and 100%; patch locations $x^p/l = 0{\cdot}1$, $0{\cdot}2$, $0{\cdot}3$, and $0{\cdot}5$ respectively. Comparisons of Table 3 show an excellent match between Lall's and the present method. Such results are expected since both methods are based on the Rayleigh–Ritz approach. Chief advantage of the proposed formulation, however, is the ease with which mode shapes for all types of deformation in any layer can be visualized. Figure 4 shows the first three flexural modes of the beam as well as the corresponding longitudinal modes of layers 1 and 3, and shear mode of layer 2 for Rao's example [4].

5. EXPERIMENTAL STUDIES

In order to further verify the analytical model as well as to investigate various phenomena associated with patch damping, modal tests are carried out on a cantilever beam made of mild steel (Table 4). A periodic "chirp" as generated within the signal analyzer is fed to a non-contacting magnetic transducer that excites the beam at the free

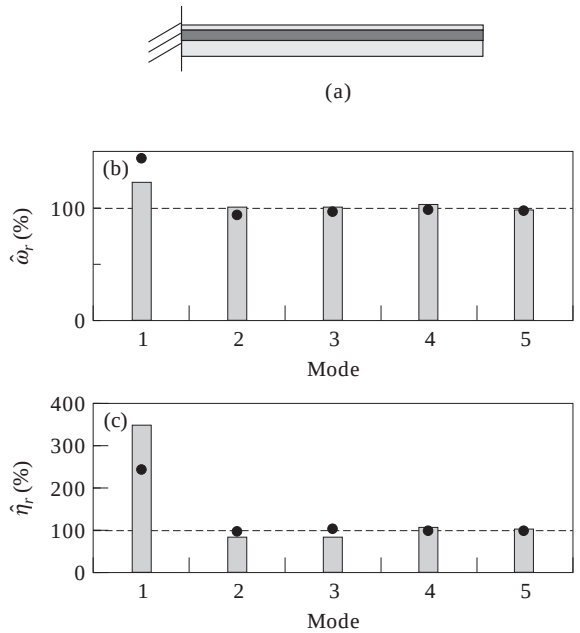

Figure 11. Results for a cantilever beam with fixed-end patch. (a) Schematic, (b) normalized eigenvalues, (c) normalized modal loss factors. Key: □, experiment; ●, theory; --, benchmark (measured value for a free-end patch).

end, as shown in Figure 5. Structural response is measured via a compact accelerometer (of weight 1 g) near the root. Sinusoidal transfer functions are then obtained. No calibration is necessary since only frequency measurements are needed. First five natural frequencies (f_r) and modal loss factors (η_r) are then extracted using the half-power bandwidth method [1].

Two types of damping treatment (designated here as Patches A and B) with material properties and layer thickness as specified in Table 4 are applied in these studies. However, the material properties of the viscoelastic core are not available. Therefore, a process for estimating the material properties must be developed before analyzing the damped beam structure. An uncertainty study is also carried out to establish error bounds for estimations. Finally, the procedure used for obtaining normalized expressions is explained in this section.

5.1. MATERIAL PROPERTY ESTIMATION

A material property estimation technique is employed by combining analytical predictions and measured modal results. Of interest here are the properties of layer 2: G_2 and η_2 since layers 1 and 3 are made of well-known steel. The following procedure is demonstrated with Patch A as an example:

(1) Choose one example and perform an experiment. The example case is a cantilever beam with full damping treatment on one side and free patch boundary at $x = 0$ as shown in Figure 6(a). Natural frequencies and modal loss factors for the first few modes are then obtained as listed in Table 5.

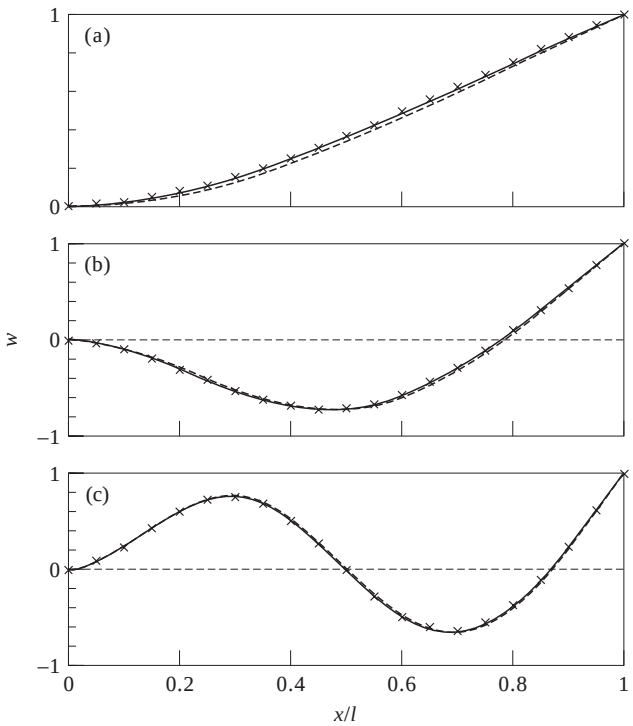

Figure 12. Flexural displacement mode shapes. (a) Mode 1, (b) mode 2, (c) mode 3. Key: ——, free-end patch; ×, fixed-end patch; · · ·, baseline beam.

(2) Develop f_r–G_2 relationships where $f_r = \omega_r / 2\pi$ is the natural frequency in Hz. With the material loss factor η_2 taken as zero, the analytical model is used to predict the variation in f_r over a range of G_2 values. A general trend of this relationship can be seen in Figure 7, where three distinct regions are observed: very compliant, transition and very stiff. These are similar to those reported in beams with joints [12].

(3) Given measured f_r results, find shear modulus G_2 from the graphs. In Figure 7, a horizontal line is drawn at the measured frequency for each mode. A cross mark represents the intersection of this line and the f_r–G_2 curve; this yields G_2 at that frequency. Note that in Figure 7(a), no intersection is found because the measured value is less than the low frequency asymptote of the curve. This is because of the non-ideal clamping boundary conditions [13], which especially affect mode 1. Therefore, mode 1 is excluded from the shear modulus estimation procedure. Figure 7(b–e) show similar G_2 values over the range of interest. For this particular case, it is safe to assume a spectrally invariant G_2, as listed in Table 4.

(4) Develop η_r–η_2 relationships and estimate the material loss factor of layer 2 as a function of frequency. With the assumed G_2 or $G_2(f)$, the analytical model is again used to predict a general relationship between η_2 and the modal loss factors η_r of the sandwich beam. In Figure 8, such η_r–η_2 relationships are compared with the measured modal loss factors. Again, each cross mark indicates the η_r value. As a result, a frequency dependent relationship is obtained for the viscoelastic core of Patch A that is curve fitted to yield:

$$\eta_{2,A}(f) = 8{\cdot}78 \times 10^{-1} + 3{\cdot}94 \times 10^{-3} f + 4{\cdot}34 \times 10^{-6} f^2 - 6{\cdot}65 \times 10^{-9} f^3 + 2{\cdot}29 \times 10^{-12} f^4,$$

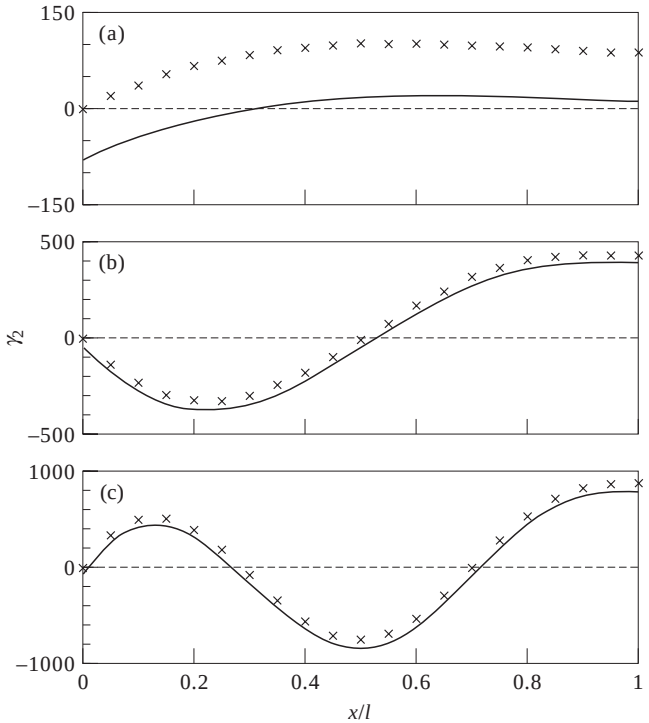

Figure 13. Shear deformation mode shapes of layer 2. (a) Mode 1, (b) mode 2, (c) mode 3. Key: ——, free-end patch; ×, fixed-end patch.

where f is the frequency in Hz. The same procedure is performed on Patch B and the material loss factor is expressed as

$$\eta_{2,B}(f) = 2{\cdot}39 \times 10^{-1} + 3{\cdot}54 \times 10^{-4} f - 7{\cdot}97 \times 10^{-7} f^2 + 1{\cdot}01 \times 10^{-9} f^3 - 3{\cdot}32 \times 10^{-13} f^4.$$

With given material properties as listed in Table 4, a specific eigenvalue problem may be constructed for each mode with a particular η_2 value at the natural frequency. An iterative procedure is obviously needed for obtaining eigensolutions [9]. Nonetheless, despite their frequency dependent nature, the material loss factors are assumed to be invariant in the immediate vicinity of an eigenvalue to avoid any iteration [10]. Experimental results that will be reported in the next section validate this assumption. Also note that the analytical formulation is again used with 20 admissible functions and 20 trial functions for all example cases.

5.2. UNCERTAINTY OF MATERIAL PROPERTY

The determination of η_2 is a key to the success of analytical method of the article. However, modal measurements used for the estimation procedure are affected by many factors including inherent beam damping, microscopic friction at the root and non-perfect bindings between layers. In practical structures a significant variation in measured η_r values may be seen. To examine such uncertainties, a $\pm 20\%$ tolerance in the damping measurement is assumed. The upper and lower bounds of $\eta_{2,A}(f)$ due to this tolerance are shown in Figure 9. These values are applied to the case of Figure 10(a), where a single patch is applied to the cantilever beam from $x = 0{\cdot}3l$ to l. A comparison of predicted and measured modal loss factors is shown in Figure 10(b). Note that the error bars on predicted η_r indicate the uncertainty associated with the $\eta_{2,A}(f)$ estimation, while the error

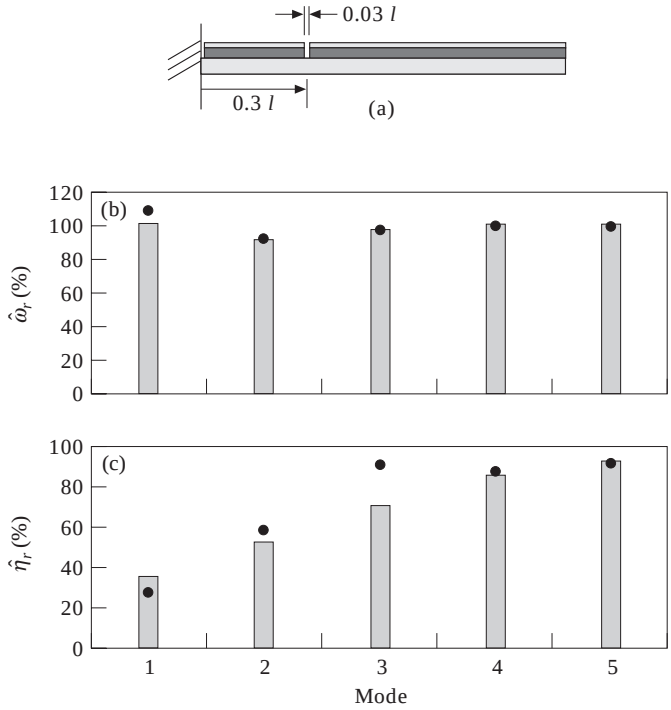

Figure 14. Results for a cantilever sandwich beam with a small cutout. (a) Schematic with a free-end patch, (b) normalized eigenvalues, (c) normalized modal loss factors. Key: □ , experiment; ●, theory.

bars on experimental results indicate the 20% tolerance in measurements. The overlap of error bars implies excellent agreement between measurements and predictions. Only the mean values of η_2 are used in subsequent studies; however the probabilistic nature of damping values must be considered when viewing all results.

5.3. NORMALIZATION PROCEDURES

Often it is desirable to express modal results in normalized forms. For example, the loss factors of a beam with patch damping (η_r) may be normalized with respect to the case where the beam is fully covered with a viscoelastic material ($\eta_{r,full}$):

$$\hat{\eta}_r = \eta_r / \eta_{r,full} \tag{35}$$

in which both values are either predicted or measured. This normalization (given by superscript $\hat{}$) can be used to describe the effectiveness of the patch damping concept. Similarly, natural frequencies may be normalized as follows to indicate the mass loading effect

$$\hat{\omega}_r = \omega_r / \omega_{r,full}. \tag{36}$$

However, since different types of patches and boundary conditions will be discussed later, it is more appropriate to use a single set of measured results throughout the article as the base for normalization. The resulting normalized natural frequency $\hat{\omega}_r$ and modal loss factor $\hat{\eta}_r$ are defined here as

$$\hat{\eta}_{r,\mathrm{b}} = \eta_r / \eta_{r,\mathrm{b}}, \qquad \hat{\omega}_{r,\mathrm{b}} = \omega_r / \omega_{r,\mathrm{b}} \tag{37, 38}$$

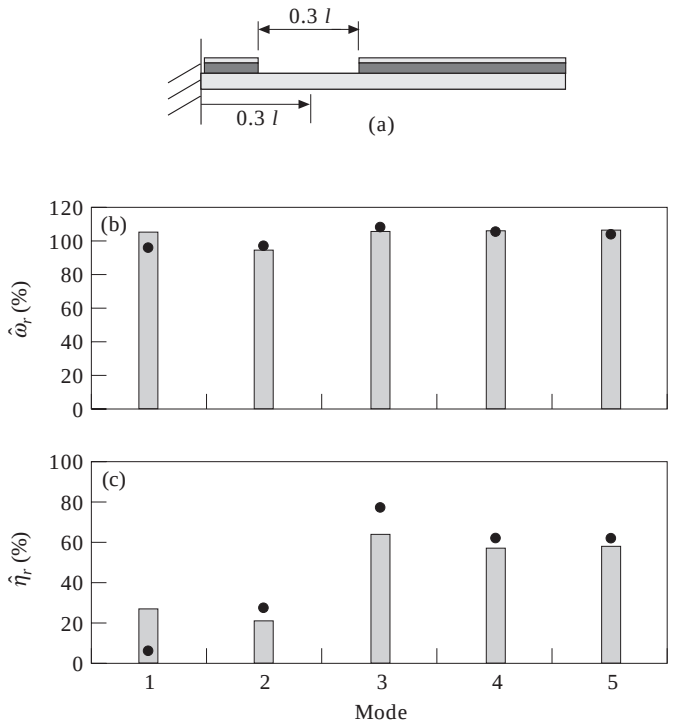

Figure 15. Results for a cantilever sandwich beam with a large cutout. (a) Schematic with a free-end patch, (b) normalized eigenvalues, (c) normalized modal loss factors. Key: □, experiment; ●, theory.

where subscript b refers to the measured results of a benchmark case: a cantilever beam with full material A damping treatment and free patch end at $x = 0$ as shown in Figure 6(a).

Yet another expression is used to describe the dimensionless eigenvalue by assuming the damped structure to be an undamped Euler beam. This eigenvalue parameter $(\beta_r l)^2$ is defined as

$$(\beta_r l)^2 = \omega_r l^2 / \sqrt{E_3 / \rho_3}. \tag{39}$$

Measured and predicted modal results for the benchmark case as well as the baseline beam (i.e., undamped beam without any damping patch) of Figure 6 are listed in Table 5. Measurements show that fairly high inherent damping is present in the first mode of the baseline beam. This may be the result of a non-ideal clamping condition at $x = 0$. Consequently, some caution must be exercised when examining the damped beam results especially at the first mode.

6. RESULTS AND DISCUSSION

6.1. EFFECT OF PATCH BOUNDARY

A cantilever beam with a damping patch embedded into the fixed boundary at $x = 0$ is said to have a fixed-end patch (Figure 3) as opposed to the free-end patch where the material is unconstrained at $x = 0$. Practically, this boundary condition is achieved by clamping the patch along with the beam at the root. Analytically, a fixed patch end is

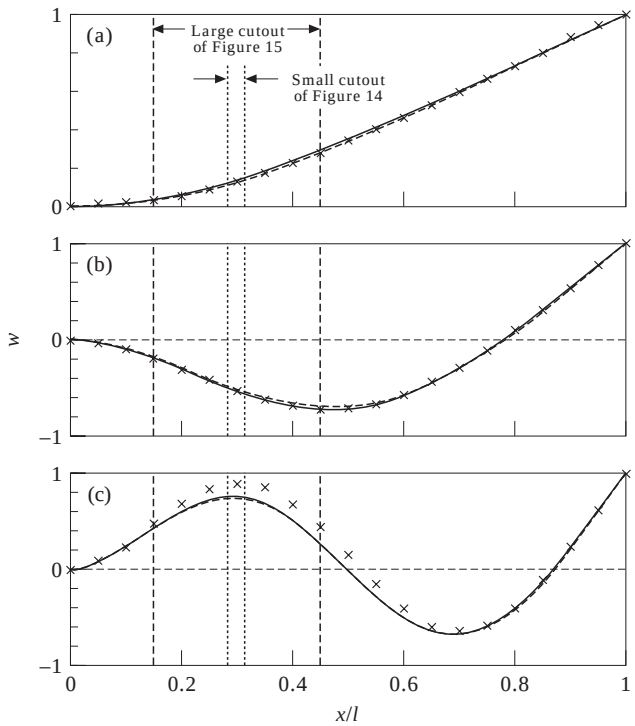

Figure 16. Flexural displacement mode shapes. (a) Mode 1, (b) mode 2, (c) mode 3. Key: ——, small cutout; ×, large cutout; --, baseline beam.

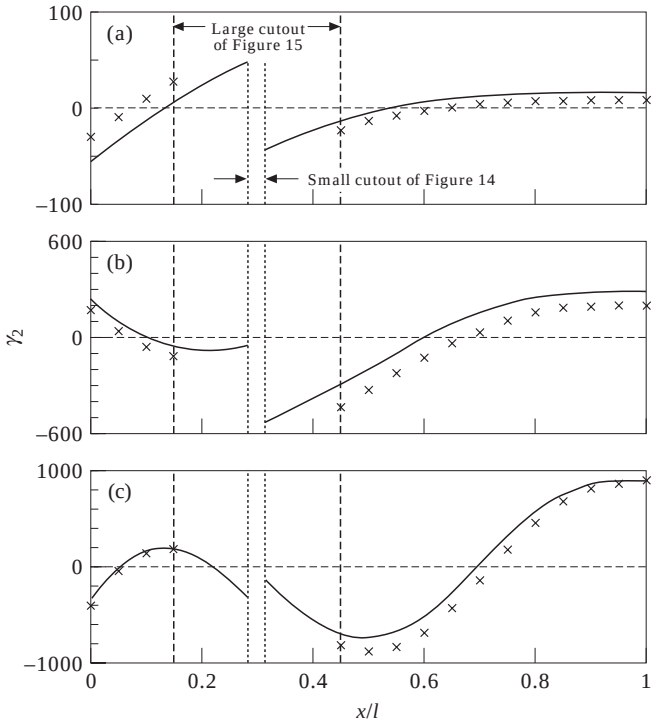

Figure 17. Shear deformation mode shapes of layer 2. (a) Mode 1, (b) mode 2, (c) mode 3. Key: ——, small cutout; ×, large cutout; --, baseline beam.

simulated by forcing the column vector $\mathbf{d}^p$ to be zero as described in section 3. Measured and predicted modal characteristics are then normalized and compared with the benchmark case (free-end patch) as shown in Figure 11.

Both measurements and predictions indicate that natural frequencies and loss factors of the beam with fixed-end patch are much higher than those of the beam with a free-end patch, especially for mode 1. Nearly coincident flexural mode shapes (Figure 12) of these two cases, as predicted by analytical models, provide little explanation for this. However, a closer examination of the shear deformation mode shapes of layer 2, as seen in Figure 13, yields very distinct characteristics between these two cases. The fixed-end patch, acting as an additional constraint, causes the natural frequencies to increase and forces the deformation γ_2 to be zero at the root. This constraint also results in a higher γ_2^2 value when

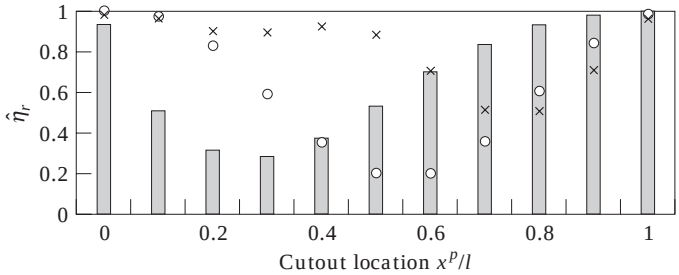

Figure 18. Effect of cutout locations on normalized loss factors of a sandwich beam. Key: □, mode 1; ○, mode 2; ×, mode 3.

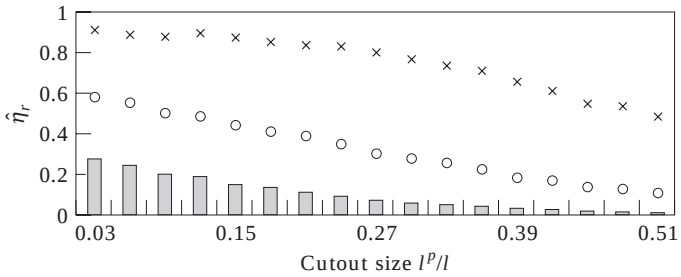

Figure 19. Effect of cutout size on normalized loss factors of a sandwich beam. Key: ▭, mode 1; ○, mode 2; ×, mode 3.

integrated over the patch length, which implies more energy dissipation. This discrepancy in shear deformation mode shapes is very noticeable for mode 1, but not as significant for modes 2 and 3 as shown in Figure 13.

6.2. EFFECT OF CUTOUTS IN DAMPING TREATMENT

A cutout, no matter how small it is, essentially creates a beam with two distinct damping patches. Resulting modal characteristics are investigated by using two example cases. Figure 14(a) shows a cantilever sandwich beam with a small cutout (with 3% of beam length) located at $0{\cdot}3l$ from the root ($x = 0$). Figure 15(a) shows a similar beam except that the cutout is 30% of the beam length but still located at $0{\cdot}3l$.

Measured and predicted eigenvalues and modal loss factors are normalized and plotted in Figures 14 and 15. It is observed that the small cutout case yields more damping than the large cutout one, as one would intuitively expect. A higher flexural amplitude is found near the cutout location of the large cutout case, especially for the third mode (Figure 16). Figure 17 shows shear deformation mode shapes in the core material. Note that a higher γ_2^2 value, when integrated over the patch length, indicates increased energy dissipation.

Parametric studies are carried out analytically in order to further investigate the effect of cutout size and cutout location. Figure 18 shows normalized loss factors of the first three modes for a sandwich beam with a 3% cutout at various locations x^p/l. It is seen that the loss factor value is very sensitive to the cutout location, especially for lower modes. Modal loss factors as affected by cutout size with a given cutout location ($0{\cdot}3l$ from the root) are

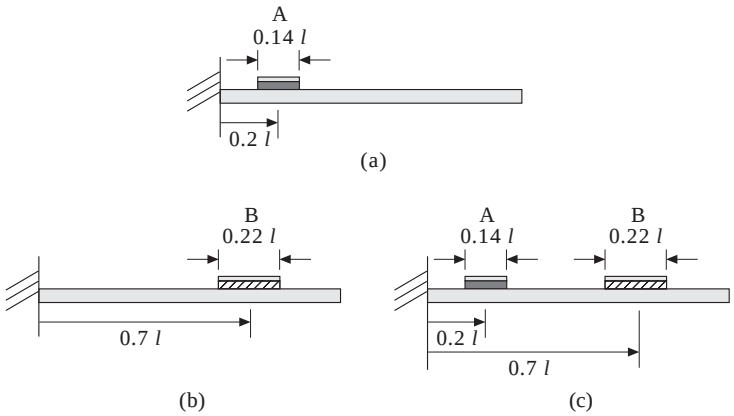

Figure 20. Cantilever beam with mismatched patches. (a) Case A, (b) Case B, (c) Case C. Note that Case C is a combination of Cases A and B.

plotted in Figure 19. Again, a monotonic decrease in η_r is observed as the cutout size is increased.

6.3. EFFECT OF TWO MISMATCHED PATCHES

A cantilever beam with two mismatched patches is examined by using three example cases, as shown in Figure 20, to see whether the damping patches introduce damping in an additive manner. A beam with a single Patch A of length $0{\cdot}14l$ located at $0{\cdot}2l$ from the root is designated as Case A, and a beam with a single Patch B of $0{\cdot}22l$ at $0{\cdot}7l$ from the root as Case B. Then both patches A and B are applied simultaneously; this is designated as Case C. Measured and predicted eigenvalues and loss factors are normalized and listed in Table 6. Flexural displacement mode shapes are shown in Figure 21.

A simple additive effect in modal damping can be expressed as

$$\eta_{r,\mathrm{C}} = \eta_{r,\mathrm{A}} + {}_r\,\eta_{r,\mathrm{B}}, \tag{40}$$

where subscripts A, B and C are the case designations defined earlier. According to the analytical model, equation (40) may not work since the resulting mode shapes are not the same because of the mass loading effect. Therefore, a modified expression is introduced to describe the additive effect as

$$\eta_{r,\mathrm{C}} = \alpha_r\,\eta_{r,\mathrm{A}} + \beta_r\,\eta_{r,\mathrm{B}}, \tag{41}$$

where α_r and β_r are the weighting factors for mode r. Note that α_r and β_r are obtained analytically and sample values are listed in Table 7. It is seen that $\alpha_r \cong 1$ and $\beta_r > 1$. This indicates that Patch B provides more damping in Case C than it does in Case B. This may be explained by looking at the shear deformation mode shapes of layer 2 in Figure 22, where γ_2 of Case C has higher absolute values in the Patch B region than that in the Patch B region of Case B.

TABLE 6

Results for a cantilever beam with mismatched patches. Refer to Figure 20

	Eigenvalue $(\beta_r l)^2$		Normalized loss factor $\hat{\eta}_r$	
Mode	Theory	Experiment	Theory (%)	Experiment (%)
(a) Beam with Patch A (Case A)				
1	3·6	3·5	1·6	23·8
2	21·7	21·5	0·0	0·6
3	58·9	58·2	1·1	1·5
4	115·1	113·7	4·1	3·2
5	193·5	189·0	4·7	3·2
(b) Beam with Patch B (Case B)				
1	3·4	3·1	0·3	14·7
2	22·0	22·0	2·4	2·6
3	61·3	61·7	6·6	5·7
4	119·3	117·8	5·6	5·5
5	195·2	188·1	3·2	3·2
(c) Beam with Patches A and B (Case C)				
1	3·4	3·2	2·0	26·4
2	21·8	21·6	2·9	2·6
3	59·1	58·8	9·2	6·6
4	114·3	113·8	12·5	8·8
5	189·2	184·7	8·8	5·5

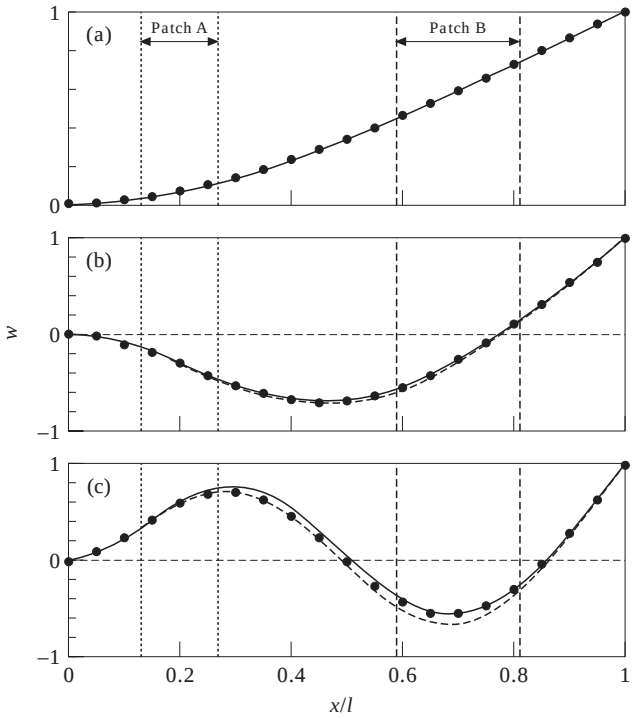

Figure 21. Flexural displacement mode shapes. (a) Mode 1, (b) mode 2, (c) mode 3. Key: · · ·, beam with Patch A; ——, beam with Patch B; ●, beam with Patches A and B.

Additionally, the issue of inherent damping in the experimental study needs to be resolved. Measured modal loss factors are considered to have contributions from inherent damping of baseline beam and applied patch damping, i.e.,

$$\eta_{r,\mathrm{AI}} = \eta_{r,\mathrm{I}} + \eta_{r,\mathrm{A}}, \qquad \eta_{r,\mathrm{BI}} = \eta_{r,\mathrm{I}} + \eta_{r,\mathrm{B}}, \qquad \eta_{r,\mathrm{CI}} = \eta_{r,\mathrm{I}} + \eta_{r,\mathrm{C}}, \tag{42a–c}$$

where the subscript I indicates the inherent damping. The values of inherent damping $\eta_{r,\mathrm{I}}$ are found from the modal measurements on the baseline beam. Modal damping of Case C is then estimated with weighting factors similar to equation (39) as

$$\eta_{r,\mathrm{CI}} = \eta_{r,\mathrm{I}} + \alpha_r \eta_{r,\mathrm{A}} + \beta_r \eta_{r,\mathrm{B}} = \eta_{r,\mathrm{I}} + \alpha_r (\eta_{r,\mathrm{AI}} - \eta_{r,\mathrm{I}}) + \beta_r (\eta_{r,\mathrm{BI}} - \eta_{r,\mathrm{I}}). \tag{43}$$

Note that one may also develop a simple additive estimation procedure where $\alpha_r = \beta_r = 1$. Modal loss factors that specifically exclude inherent damping for Cases A and B are

TABLE 7

Weighting factors α_r and β_r for equation (41) *as derived from analytical models*

Mode r	α_r	β_r
1	1·01	1·30
2	1·02	1·21
3	0·99	1·23
4	0·96	1·55
5	1·03	1·24

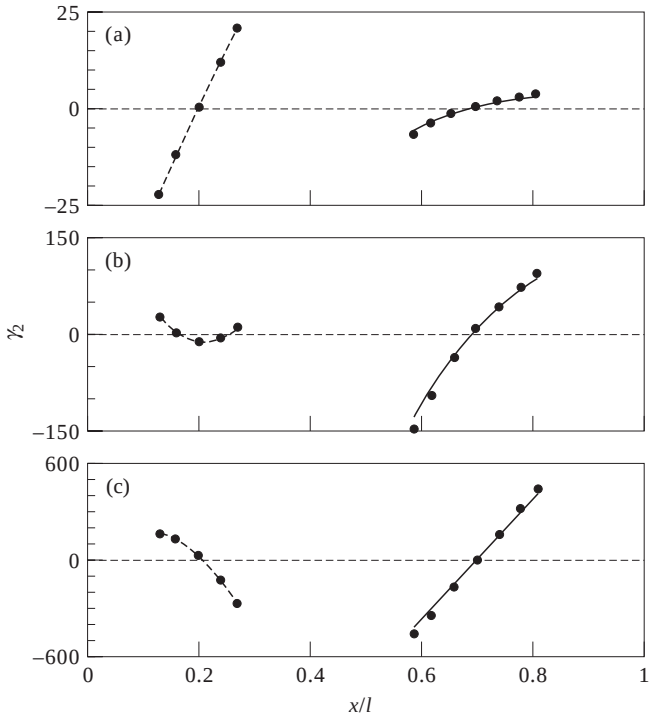

Figure 22. Shear deformation mode shapes of layer 2. (a) Mode 1, (b) mode 2, (c) mode 3. Key: · · ·, beam with Patch A; ——, beam with Patch B; ●, beam with Patches A and B.

normalized and listed in Table 8 (a). The values of $\hat{\eta}_{r,\mathrm{CI}}$ are first estimated by using equation (41) with α_r and β_r taken from the analytical results (Table 7) and then with $\alpha_r = \beta_r = 1$. Both sets of estimations (weighted and simple additive) are then compared with measured results of Case C. Table 8 (b) shows that both estimation methods compare well with measurements. Similar studies can be carried out on other patch patterns.

TABLE 8

Comparison between estimated and measured $\hat{\eta}_{r,CI}$ for the example of Figure 20

Mode r	$\hat{\eta}_{r,\mathrm{I}}$ (%)	$\hat{\eta}_{r,\mathrm{A}} = \hat{\eta}_{r,\mathrm{AI}} - \hat{\eta}_{r,\mathrm{I}}$ (%)	$\hat{\eta}_{r,\mathrm{B}} = \hat{\eta}_{r,\mathrm{BI}} - \hat{\eta}_{r,\mathrm{I}}$ (%)
(a) Estimation of $\hat{\eta}_{r,\mathrm{A}}$ and $\hat{\eta}_{r,\mathrm{B}}$			
1	14·9	8·9	0·0
2	0·5	0·2	2·1
3	0·3	1·1	5·3
4	0·5	2·8	5·0
5	0·6	2·6	2·6
Mode r	$\hat{\eta}_{r,\mathrm{CI}} = \hat{\eta}_{r,\mathrm{I}} + \hat{\eta}_{r,\mathrm{A}} + \hat{\eta}_{r,\mathrm{B}}$ (%)	$\hat{\eta}_{r,\mathrm{CI}} = \hat{\eta}_{r,\mathrm{I}} + \alpha\hat{\eta}_{r,\mathrm{A}} + \beta\hat{\eta}_{r,\mathrm{B}}$ (%)	Measured $\hat{\eta}_{r,\mathrm{CI}}$ (%)
(b) Comparison of estimated and measured $\hat{\eta}_{r,\mathrm{CI}}$			
1	23·8	23·9	26·4
2	2·8	3·2	2·6
3	6·8	8·0	6·6
4	8·3	10·9	8·8
5	5·8	6·6	5·5

7. CONCLUSION

This paper presents a refined method for analyzing the harmonic response of beams with multiple constrained-layer viscoelastic patches. Initially the method is developed for thick beams, but subsequently it is restricted to thin beams. The classic sandwich beam theory and a secondary minimization scheme are employed to derive kinematic relationships between flexural displacement and other deformations in all layers. This approach requires the inclusion of only flexural shape functions in the complex eigenvalue problem. Nonetheless, eigenvectors can be related to flexural, longitudinal and shear mode shapes, some of which can not be experimentally measured. Most important of all, the knowledge of shear deformation modes in the viscoelastic core provides an improved understanding of the effect of patch damping.

The proposed model can be applied to either fully or partially covered sandwich beams. It is successfully validated by comparing results with the examples described by Rao [7] and Lall *et al*. [4]. Several damping configurations are then experimentally and analytically studied. Excellent agreement between theory and experiment is seen for all examples. Some important patch damping issues have been clarified especially through an examination of modal deformations. In order to identify the unknown properties of the viscoelastic material used in this article, an estimation procedure has been proposed. The frequency-dependent material loss factor and stiffness are estimated by combining analytical parametric studies with modal measurements from beam tests. An uncertainty study has also been carried out to establish the error bounds of these estimations.

Future work will extend this formulation to thick beams and plates. Important design issues, including the optimization of patch patterns for improved damping performance, also need to be investigated.

ACKNOWLEDGMENT

This research has been supported by the Army Research Office (URI Grant DAAL 03-92-G-0120; 1992–97; Project monitor: Dr. T. L. Doligalski).

REFERENCES

1. A. D. Nashif, D. I. G. Jones and J. P. Henderson 1985 *Vibration Damping*. New York: John Wiley.
2. C. T. Sun and Y. P. Lu 1995 *Vibration Damping of Structural Elements*. New Jersey: Prentice Hall.
3. D. S. Nokes and F. C. Nelson 1968 *Shock and Vibration Bulletin* **38**, part 3, 5–10. Constrained layer damping with partial coverage.
4. A. K. Lall, N. T. Asnani and B. C. Nakra 1988 *Journal of Sound and Vibration* **123**, 247–259. Damping analysis of partially covered sandwich beams.
5. H. Dewa, Y. Okada and B. Nagai 1991 *JSME International Journal Series III* **34**, 210–217. Damping characteristics of flexural vibration for partially covered beams with constrained viscoelastic layers.
6. C. Levy and Q. Chen 1994 *Journal of Sound and Vibration* **177**, 15–29. Vibration analysis of a partially covered, double sandwich-type, cantilever beam.
7. D. K. Rao 1978 *Journal of Mechanical Engineering Science* **20**, 271–282. Frequency and loss factors of sandwich beams under various boundary conditions.
8. E. M. Kerwin. Jr. 1959 *Journal of the Acoustical Society of America* **31**, 952–962. Damping of flexural waves by a constrained viscoelastic layer.
9. R. M. Lin and M. K. Lim 1996 *Journal of the Acoustical Society of America* **100**, 3182–3191. Complex eigensensitivity-based characterization of structures with viscoelastic damping.
10. R. Rikards, A. Chate and E. Barkanov 1993 *Computers and Structures* **47**, 1005–1015. Finite element analysis of damping the vibration of laminated composites.

11. P. TROMPETTE, D. BOILLOT and M.-A. RAVANEL 1978 *Journal of Sound and Vibration* **60**, 345–350. The effect of boundary conditions on the vibration of a viscoelastically damped cantilever beam.
12. R. SINGH, M. L. LIAW, J. E. FARSTAD and S.-W. KUNG 1995 *The American Society of Mechanical Engineers*. Paper No. 95-WA/NCA-28. Determination of joint stiffness through vibration analysis of beam assemblies.
13. H. VINAYAK and R. SINGH 1996 *Journal of Sound and Vibration* **192**, 741–769. Eigensolutions of annular-like elastic disks with intentionally removed or added material.

APPENDIX A: LIST OF SYMBOLS

A	cross sectional area
$\mathbf{A}$	governing equation matrix
$\mathbf{a}$, $\mathbf{b}$, $\mathbf{c}$	coefficient vectors
a, b, c	coefficients
$\mathbf{B}$	governing equation vector
$\mathbf{C}$	coefficient vector
C	thickness parameter $(h_1 + 2h_2 + h_3)/2$
$\mathbf{d}$	spatial matrix
d	spatial constant
$\mathbf{E}$	elasticity matrix
E	Young's modulus
e	elasticity ratio $E_3 A_3 / E_1 A_1$
f	frequency (Hz)
G	shear modulus
$\mathbf{H}$	inertia matrix
h	thickness
I	area moment of inertia
i	$\sqrt{-1}$
$\mathbf{K}$	stiffness matrix
l	length
$\mathbf{M}$	mass matrix
N	total number of patches
n	total number of shape functions
$\mathbf{q}$	generalized displacement vector
q	generalized displacement
$\mathbf{r}$	deformation vector
$\mathbf{S}$	admissible shape function matrix
T	kinetic energy
u	in-plane or longitudinal displacement
U	potential or strain energy
$\mathbf{V}$	transfer matrix
w	flexural displacement
x, z	spatial coordinates
γ	shear deformation
η	loss factor
κ	shear correction factor
λ	eigenvalue
$\boldsymbol{\xi}$	rotational shape function vector
ξ	rotational shape function
ρ	mass density
$\boldsymbol{\varsigma}$	longitudinal shape function vector
ς	longitudinal shape function
$\boldsymbol{\Phi}$	reduced admissible shape matrix
$\boldsymbol{\varphi}$	flexural shape function vector
ϕ	flexural shape function
$\boldsymbol{\chi}$	trial function vector for longitudinal displacement
$\boldsymbol{\psi}$	rotation vector
ψ	rotation
ω	frequency (rad/s)

OPERATORS

$\mathscr{D}$	differential operator matrix
Im	imaginary part
Re	real part
ϑ	a spatial operator
∂	differential operator

SUPERSCRIPTS

p	patch number
T	transpose
$\tilde{}$	complex valued
$\hat{}$	normalized quantity

SUBSCRIPTS

A, B	type of damping patch
b	measurement of the benchmark case
I	inherent damping
i	layer number
k	admissible function number
r	modal index
1	layer 1 (elastic constraining layer)
2	layer 2 (viscoelastic constrained layer)
3	layer 3 (base structure: beam)